Performance of Supervised Classification Algorithms of Hyperspectral Imagery for Identifying Fecal and Ingesta Contaminants

B. Park, K. C. Lawrence, W. R. Windham, D. P. Smith

Abstract. *In order to select the optimum classifier, the performance of six different supervised classification algorithms including parallelepiped, minimum distance, Mahalanobis distance, maximum likelihood, spectral angle mapper, and binary coding were investigated and compared for identifying fecal and ingesta contaminants in hyperspectral poultry imagery. A pushbroom line-scan hyperspectral imager was used for hyperspectral image acquisition, with 512 narrow bands between 400 and 900 nm wavelengths. Three different feces from digestive tracts (duodenum, ceca, colon) and ingesta were considered as contaminants. These contaminants were collected from broiler carcasses that had been fed a mixture of corn, milo, or wheat with soybean. The classification accuracies varied from 62.9% to 92.3% depending on the classification method. The highest classification accuracy for identifying contaminants from corn-fed carcasses was 92.3% with a spectral angle mapper classifier. The accuracy was 82.1% with the maximum likelihood method for milo-fed carcasses, and 91.2% accuracy was obtained for wheat-fed carcasses when the same classification method was employed. The mean classification accuracy for classifying fecal and ingesta contaminants obtained in this study was 90.3%.*

Keywords. *Classification, Fecal contamination, Food safety inspection, Hyperspectral, Image classification, Imaging spectroscopy, Poultry.*

Food safety is an important issue for public health, and reductions in the potential health risks to consumers from human pathogens in food are crucial. About 9,000 deaths and 6.5 to 33 million illnesses in the U.S. each year are food-related. The USDA estimates that medical costs and productivity losses for seven specific pathogens in food range between $6.5 billion and $34.9 billion annually. Total costs for all foodborne illnesses are likely to be much higher (FSIS, 1997).

In 1995, the USDA Food Safety and Inspection Service (FSIS) inspected more than 7 billion poultry carcasses. The task of inspecting meat and poultry is imposing because consumers spend $120 billion, or one-third of their annual food dollars, for meat and poultry products. On 25 July 1996, the FSIS finalized the most significant changes in meat and poultry inspection rules. The final rule on pathogen reduction and Hazard Analysis and Critical Control Point (HACCP) systems (USDA, 1996) targets pathogens that cause foodborne illness, strengthens industry responsibility to produce safe food, and focuses inspection and plant activities on prevention objectives. The purpose of HACCP systems is to identify potential food safety hazards arising in slaughter and processing plants. HACCP is a system of steps used to identify and prevent problems from occurring during food processing and to correct them as soon as they are detected. With HACCP in place, FSIS can verify that the plant is controlling its processes and consistently producing products that comply with food safety requirements.

Poultry and poultry products are an important source of the total supply of food in the U.S. Currently, the inspection system is based largely on what inspectors can see: diseases, defects, and contamination on poultry carcasses. The FSIS is changing the federal meat and poultry inspection system from a system based primarily on sight, touch, and smell to one incorporating scientific testing and systematic prevention of contamination.

It is essential to the public interest that the health and welfare of consumers be protected by ensuring that the poultry products distributed to them are wholesome. In general, fecal material color ranges from varying shades of yellow to green, brown, and white; the consistency of feces is usually semi-solid to paste; and the composition of feces may include plant materials. Inspectors use these guidelines to prevent visibly fecal-contaminated carcasses from entering the chilling tanks.

Imaging spectroscopy or hyperspectral imaging, in reference to the multispectral characteristics of the data set, refers to the imaging of a scene over a large number of discrete, contiguous spectral bands such that a complete reflectance spectrum can be obtained for the region being imaged. The reflectance spectra from the surface of food materials contain characteristic or diagnostic absorption features. Reflectance spectral features can be used to identify a number of

Submitted for review in March 2006 as manuscript number IET 6414; approved for publication by the Information & Electrical Technologies Division of ASABE in September 2006.

The authors are **Bosoon Park, ASABE Member Engineer,** Agricultural Engineer, **Kurt C. Lawrence, ASABE Member Engineer,** Agricultural Engineer, **William R. Windham,** Research Leader, and **Douglas P. Smith,** Research Food Technologist, USDA-ARS Richard B. Russell Research Center, Athens, Georgia. **Corresponding author:** Bosoon Park, USDA-ARS Richard B. Russell Research Center, P.O. Box 5677, Athens, GA 30604-5677; phone: 706-546-3396; fax 706-546-3633; e-mail: bosoon.park@ars.usda.gov.

important spectral characteristics of surface contaminants such as feces.

Hyperspectral imaging has emerged as a powerful technique in agricultural and food systems for such applications as vegetation assessment (Bostater, 1998); determining fruit ripeness (Polder et al., 2000), sugar content in melon (Tsuta et al., 2002), and apple bruise (Lu et al., 1999); wheat scab inspection (Delwiche and Kim, 2000); and food safety (Park et al., 2003a; Lawrence et al., 2003; Windham et al., 2003; Kim et al., 2001). Applications in other fields include medical imaging (Levenson et al., 1998; Burman, 1999; Dwyer and DiMarzio, 1999; Malkoff and Oliver, 2000; Huebschman et al., 2002; Zuzak et al., 2002), biological imaging (Feyaerts et al., 1999; Arnoldussen et al., 2000; Inoue et al., 2001; Spillman et al., 2001), industrial applications (Willoughby et al., 1996), and earth remote sensing (Schowengerdt, 1997; Hart et al., 1998). Thus, hyperspectral imaging is an extremely useful tool to thoroughly analyze the spectra of inhomogeneous materials that contain a wide range of spectral and spatial information.

Therefore, hyperspectral imagery can be an effective technique for identifying surface contaminants on poultry carcasses (Park et al., 2003a; Windham et al., 2003). Previously, hyperspectral and multispectral imaging techniques have been applied to detect fecal contaminants on the surface of poultry carcasses (Park et al., 2003a; Lawrence et al., 2003; Windham et al., 2003). However, in order to successfully implement hyperspectral imaging techniques for HACCP, each contaminant needs to be identified to minimize production of contaminated carcasses during processing. The objective of this research is to investigate various classification methods to determine the optimum classifiers to identify fecal and ingesta contaminants on broiler carcasses. The specific objective includes investigating six supervised classifiers to differentiate fecal types based on three different diets commonly used in the poultry industry.

Materials and Methods

Materials

Broilers were obtained from a commercial growout house, transported to the University of Georgia's research farm, and placed into broiler research housing. On each of eight days, 29 birds were selected for processing. Birds were then caught, cooped, and transported to the processing facility. Prior to slaughter, birds were electrically stunned for 12 s at 50 VAC (approx. 25 mA), necks were manually cut, and birds were bled for 120 s. Carcasses were scalded at 53°C for 120 s in a batch scalder with water recirculation and were picked for 30 s. Heads and feet were removed from the carcasses, and the viscera were removed manually. The gastrointestinal tract was separated into distinct area using clamps, and the contents removed from the crop and gizzard (ingesta), duodenum, ceca, and colon were kept in sample bowls until applied to the carcasses for fecal sample collection.

Hyperspectral Imaging System

A hyperspectral imaging system (Park et al., 2003a) was used to collect spectral images of contaminated and uncontaminated poultry carcasses. A transportable imaging cart was designed to provide both portability and flexibility in positioning both the lights and the camera system. The cart also contained a computer, power supplies, and other equipment for hypercube date collection. Lighting requirements were evaluated and adjusted for quality image acquisition. The imaging system consisted of an imaging spectrograph with 25 μm slit width and an effective slit lengths of 8.8 mm (Grating Type I, ImSpector V9, PixelVision, Beaverton, Ore.), a high-resolution CCD camera (SensiCam model 370KL, Cooke Corp., Auburn Hills, Mich.), a 1.4/23 mm compact C-mount focusing lens (Xenoplan, Schneider, Hauppauge, N.Y.) and associated optical hardware, a motor for lens motion control (model RSP-2T, Newport Corp., Irvine, Cal.), a frame grabber (12-bit PCI interface board, Cooke Corp., Auburn Hills, Mich.), and a computer (Pentium II, 500 MHz).

The prism-grating-prism spectrograph had a nominal spectral range of 430 to 900 nm with 6.6 mm axis and attached to the camera for generating line-scan images. The spectrograph had a nominal spectral resolution of 2.5 nm. It was connected to a 2/3-inch silicon-based CCD sensor with a 1280 by 1024 pixel resolution. The camera was thermoelectrically cooled and had a spectral response from 290 to 1000 nm with a maximum readout time of 8 fps. For consistent illumination of poultry carcasses, the lighting system consisted of the 150 W quartz halogen DC-stabilized fiber optic illuminator (Fiber-Lite A240, Dolan-Jenner, Inc., Lawrence, Mass.) with lamp assembly, fiber optic cables, and quartz halogen line lights of 10-inch illuminating size (QF5048, Dolan-Jenner, Inc., Lawrence, Mass.).

Classification Methods

Six supervised classification methods were examined in this study for selecting optimum classifiers to identify contaminants on the surface of broiler carcasses. Those methods were parallelepiped, minimum distance, maximum likelihood, Mahalanobis distance, spectral angle mapper, and binary encoding classifier.

Parallelepiped classification used a simple decision rule to classify hyperspectral data. The decision boundaries formed an *n*-dimensional parallelepiped in the image data space. The dimensions of the parallelepiped were defined based on a standard deviation threshold from the mean of each selected class. If a pixel value was above the low threshold and below the high threshold for all *n* bands being classified, then it was assigned to that class.

The minimum distance method used the mean vectors of each endmember and calculates the Euclidean distance from each unknown pixel to the mean vector for each class. All pixels were classified to the nearest class unless a standard deviation or distance threshold was specified, in which case some pixels were unclassified if they did not meet the selected criteria.

Maximum likelihood classification assumed that the statistics for each class in each band were normally distributed and calculates the probability that a given pixel belongs to a specific class. Unless a probability threshold was selected, all pixels were classified. Each pixel was assigned to the class that has the highest probability.

The Mahalanobis distance classification is a direction-sensitive distance classifier that uses statistics for each class. It is similar to maximum likelihood classification but assumes that all class covariances are equal; therefore, processing time is faster. All pixels were classified to the

closest region of interest (ROI) class unless a distance threshold was specified, in which case some pixels were unclassified if they do not meet the threshold. For more details about classification algorithms, see Richards and Jia (1999).

The spectral angle mapper (SAM) is a physically based spectral classification method that uses an *n*-dimensional angle to match pixels to reference spectra. The algorithm determined the spectral similarity between two spectra by calculating the angle between the spectra, treating them as vectors in a space with dimensionality equal to the number of bands. SAM compared the angle between the endmember spectrum vector and each pixel vector in *n*-dimensional space. Smaller angles represent closer matches to the reference spectrum. For more details, see Kurse et al. (1993).

Binary encoding classification encoded the data and endmember spectra into zeroes and ones based on whether a band falls below or above the spectrum mean. An exclusive-OR function was used to compare each encoded reference spectrum with the encoded data spectra, and a classification image was produced. For more details about binary encoding classification, see Mazer et al. (1988).

Procedure

Immediately after processing, the carcasses, fecal, and ingesta samples were transported to the USDA Hyperspectral Imaging Laboratory for image acquisition. Carcasses were imaged in a shackle welded to a stainless steel rod, suspended across two stands. First, hyperspectral images of uncontaminated carcasses were collected, and then carcasses were contaminated with feces and ingesta varying in type of contaminants, contaminated spot size, and location on the carcass. Pushbroom line-scan images were collected using SensiCam software based on the following control settings. Image pixels of the high-resolution CCD detector were 1280 by 1024; however, actual image size and the number of wavelength bands are defined by binning size. For our experiment, 4 by 2 binning of the line-scan image created an actual image size of 320 (horizontal) by 340 (vertical) spatial resolution with 512 wavelengths. In this case, the number of line scans, which depends on the size of the carcass and the motor speed for lens movement, was 340. For more detail on hyperspectral data acquisition, see Park et al. (2003a).

The images of carcasses (N = 29) were selected based on three different diets (a mixture of corn, milo, or wheat with soybean) from each day of processing. On each carcass image, regions of interest (ROI) were chosen manually at seven different locations (uncontaminated skin from the thigh, breast, and wing portions of the carcasses; and duodenum, ceca, colon, and ingesta contaminants applied to the carcass) for a total of 203 image ROI data sets. The ROIs of uncontaminated and contaminated skin were selected using the rectangle, polygon, and drawing point modes. When selecting the ROIs, it was attempted to make all a minimum of 50 pixels; however, when this was not possible, as many pixels as possible were chosen. In the case of fecal and ingesta ROIs, the 50 pixels were chosen from the center of the contaminant spot to avoid the edge pixels, which may have contained spectral information from sources other than the contaminant. The mean ROI reflectance spectra at each wavelength were calculated. Hyperspectral images were processed and analyzed using Environment for Visualizing Images (ENVI 3.6) software (Research Systems, Inc., Boulder, Colo.). After ROIs were obtained from each broiler carcass hyperspectral image, the individual image classification methods were applied for the identification of fecal and ingesta contaminants on the poultry broiler carcasses. For the SAM classification, the spectral library of each ROI was created and saved in advance. After all six supervised classification methods were applied to the hyperspectral ROI data, the post-classification method (a confusion matrix in this case) was applied for selection of the optimum classification method for identifying fecal and ingesta contaminants.

For the assessment of classification accuracy, a confusion matrix was analyzed to determine the accuracy of a classification method's results by comparing the results with ground truth ROI information. The kappa (κ) coefficient was also calculated to compare the accuracy of different classifiers. The κ coefficient is an indicator of the overall agreement of a matrix and accounts for all the elements in a confusion matrix. The κ coefficient can be obtained by equation 1:

$$\kappa = \frac{N \sum_{k} x_{kk} - \sum_{k} x_{k\Sigma} x_{\Sigma k}}{N^2 - \sum_{k} x_{k\Sigma} x_{\Sigma k}} \quad (1)$$

where N is the total number of pixels in all ground truth classes, x_{kk} is the sum of confusion matrix diagonals, $x_{k\Sigma}$ is the sum of ground truth pixels in a class, and $x_{\Sigma k}$ is the sum of classified pixels in that class. The κ coefficient is always less than or equal to 1. A value of 1 implies perfect agreement, and values less than 1 imply less than perfect agreement.

Results and Discussions

Hyperspectral Image ROI and Spectral Characteristics for Classification

In order to select the optimum classification method for identifying fecal and ingesta contaminants on the poultry broiler carcasses, six different supervised classification methods were investigated and the results were compared. Figure 1 shows a typical hyperspectral image of an uncontaminated carcass (fig. 1a) and surface contaminants with ROI (fig.1b). In this sample, 25 pixels were observed as duodenum, 27 pixels as ceca, 78 pixels as colon, 93 pixels as ingesta, and 195 pixels as skin (for classification, skin included thigh, breast, and wing).

Figure 2 shows the corresponding spectra of each ROI (fig. 1b). The spectra indicate duodenum, ceca, colon, ingesta, thigh, breast, and wing. Typically, the spectra from contaminants gradually increased with wavelength from 420 to 730 nm, whereas reflectance spectra of skin increased up to about 520 nm, decreased, and then increased again from about 550 nm. The reflectance spectra of skin are much higher than those of the contaminants. The reflectance spectral characteristics were similar to the results previously reported (Park et al., 2003b).

Comparison of Classification Methods

Figure 3 shows six different classification maps used to visualize the results of each classification method tested to identify fecal and ingesta contaminants on the surface of broiler carcasses. The parallelepiped classifier identified duodenum, ceca, and colon with high accuracy. However,

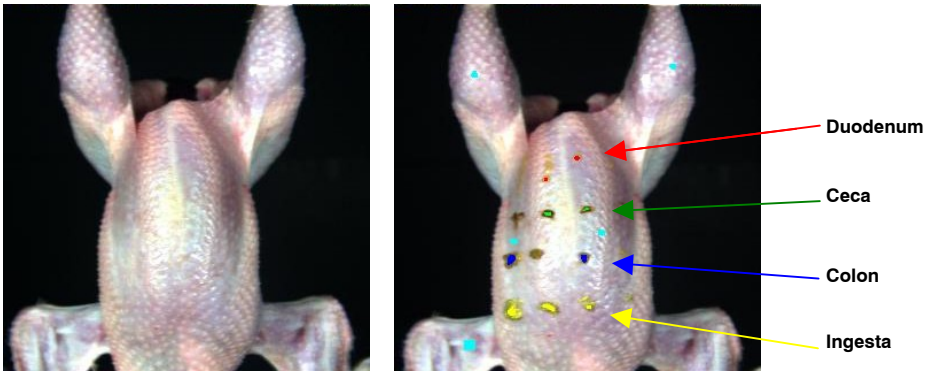

Figure 1. ROI of a corn-fed poultry carcass: (a) clean (uncontaminated) carcass, and (b) fecal contaminant ROI. Duodenum = red (25 pixels), ceca = green (27 pixels), colon = blue (78 pixels), ingesta = yellow (93 pixels), and skin = cyan (195 pixels).

many ingesta pixels were misclassified as duodenum (fig. 3a). Most duodenum, ceca, and colon contaminants, except ingesta, were also classified correctly by the minimum distance classifier (fig. 3b). The Mahalanobis distance classifier also classified fecal contaminants with high accuracy, yet most ingesta contaminants were misclassified as duodenum, and uncontaminated skin surfaces were also misclassified as duodenum (false positive) (fig. 3c). The results of the maximum likelihood classifier were similar to those of the Mahalanobis distance classifier. The duodenum, ceca, and colon contaminants were classified with minimal misclassification. The misclassification of ingesta was much lower than that of the Mahalanobis distance classifier. However, many false positive pixels for uncontaminated skin were found (fig. 3d). The spectral angle mapper classifier also identified most fecal and ingesta contaminants with high classification accuracy. However, with this classifier, many pixels in the skin and vent area were misclassified as duodenum (fig. 3e). Even though the classification accuracy was not high enough, the binary coding classifier correctly classified most fecal contaminants and ingesta as well. With this classifier, many pixels in the skin were misclassified as colon contaminants (fig. 3f).

Accuracy of Classification Methods

Six different supervised classification methods were applied to the broiler carcasses that had been fed three different diets to compare the accuracy of classification methods for selecting robust classifiers regardless of diet. Table 1 lists the classification accuracies of the methods as applied to carcasses fed a corn/soybean diet. The classification accuracies ranged from 54.6% (parallelepiped) to 99.9% (maximum likelihood). In most cases, the maximum likelihood classifier and spectral angle mapper had a higher accuracy than the other classifiers. The accuracy of the maximum likelihood classifier ranged from 75.4% to 99.9%, whereas the spectral angle mapper had classification accuracies of 83.5% to 97.8%.

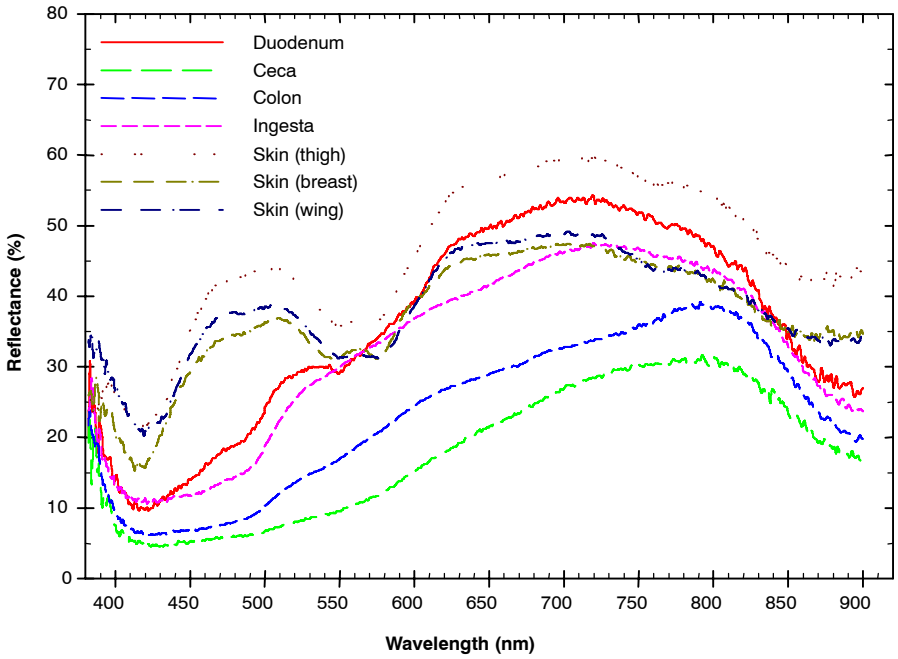

Figure 2. Mean spectra of fecal and ingesta contaminant ROIs from corn-fed poultry broiler carcass.

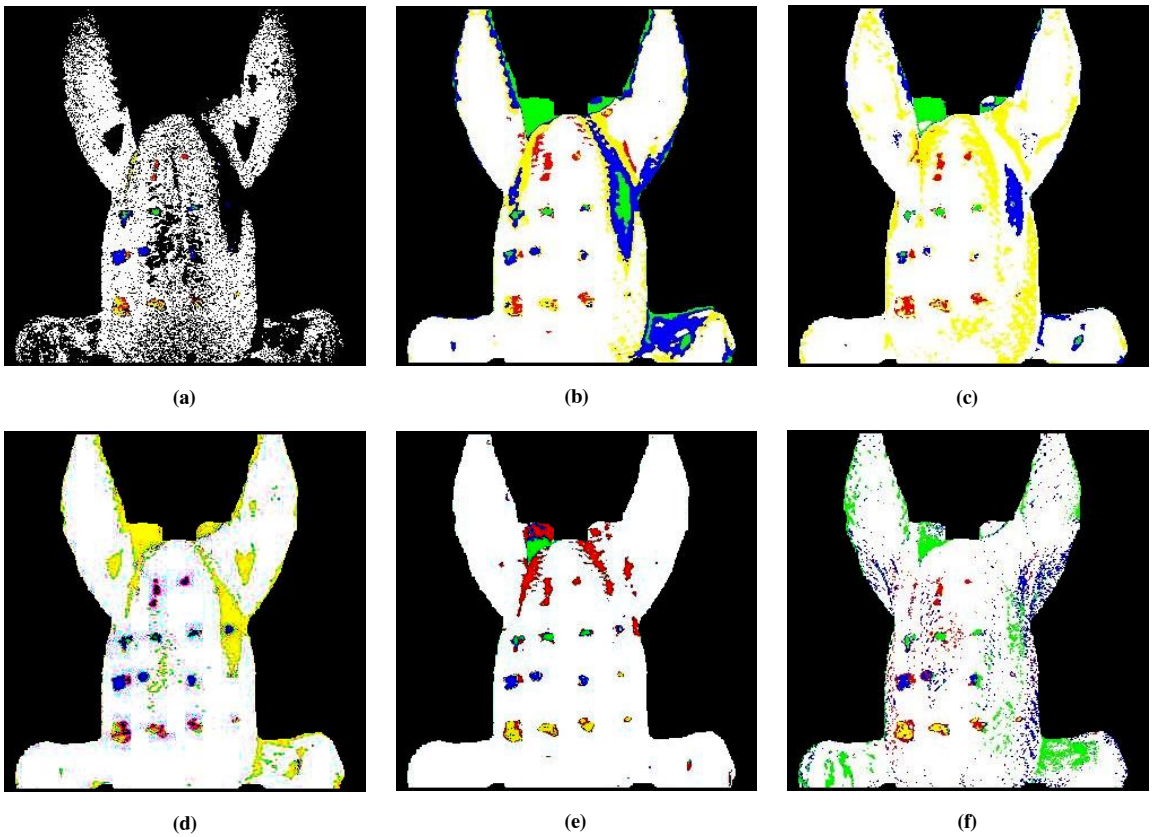

Figure 3. Classification maps from mean spectra of surface contaminant ROI on a corn-fed poultry carcass: (a) parallelepiped classifier, (b) minimum distance classifier, (c) Mahalanobis distance classifier, (d) maximum likelihood classifier, (e) spectral angle mapper classifier, and (f) binary coding classifier. Each color map represents duodenum (red), ceca (green), colon (blue), ingesta (yellow), skin (white), and unclassified or background (black). (The appearance of each contaminant on the surface is the same as in figure 1.)

Table 2 lists the accuracy of each classifier as applied to milo-fed broiler carcasses. Similar to the corn-fed carcasses, the maximum likelihood classifier and the spectral angle mapper both performed better than the other classifiers. Overall, the classification accuracy of each classifier was lower than with the corn-fed samples. The classification accuracies with milo-fed carcasses ranged from only 50% (binary coding) to 96.9% (maximum likelihood).

Table 1. Accuracy of classification methods used to classify three different feces and ingesta contaminants on corn-fed broiler carcasses.

	Sample Examined									
Method[a]	C1609f	C1621f	C1635f	C1646f	C1657f	C1670f	C1672f	C1681f	C1684f	C1693f
Par	59.09	69.02	77.63	63.02	72.12	57.14	81.11	54.59	55.05	58.26
Min	75.12	76.72	92.88	76.89	75.48	84.89	96.74	75.84	74.31	68.48
Mah	76.32	60.29	89.15	74.94	63.22	68.68	77.20	62.64	60.09	59.57
Max	75.36	91.68	**98.64**	**96.84**	**91.83**	96.98	**99.90**	81.21	89.68	**92.17**
Sam	**83.49**	**93.35**	98.31	95.38	90.87	**97.80**	98.05	**86.35**	**91.06**	88.04
Bin	57.89	66.94	77.97	62.04	75.00	68.13	77.20	57.49	57.11	68.48

[a] Par = parallelepiped, Min = minimum distance, Mah = Mahalanobis distance, Max = maximum likelihood, Sam = spectral angle mapper, and Bin = binary coding.

Table 2. Accuracy of classification methods used to classify three different feces and ingesta contaminants on milo-fed broiler carcasses.

	Sample Examined									
Method[a]	M1601f	M1613f	M1628f	M1639f	M1652f	M1661f	M1664f	M1675f	M1676f	M1685f
Par	50.47	61.73	74.59	62.88	80.17	56.04	74.76	80.44	54.04	69.70
Min	79.63	81.40	88.45	80.30	87.15	56.66	71.67	88.98	62.11	91.13
Mah	65.61	76.32	88.12	66.16	66.48	64.71	68.10	73.00	50.31	85.28
Max	88.79	89.43	**96.37**	**93.43**	**91.06**	81.73	**91.90**	**95.59**	54.97	**96.97**
Sam	**95.70**	**91.54**	91.75	82.58	86.31	**87.62**	78.10	89.53	**77.64**	92.64
Bin	70.65	59.62	76.57	58.33	69.27	54.18	64.29	61.16	50.00	65.37

[a] Par = parallelepiped, Min = minimum distance, Mah = Mahalanobis distance, Max = maximum likelihood, Sam = spectral angle mapper, and Bin = binary coding.

Table 3 lists the classification accuracies for wheat-fed broiler carcasses. Similar to the corn- and milo-fed carcasses described above, the performances of the maximum likelihood classifier and the spectral angle mapper were both higher than the other classifiers. Because of the similar color of duodenum contaminants and skin on the wheat-fed carcasses, the overall accuracy was lower than the results with the corn and milo diets. The classification accuracies ranged from 47.4% (parallelepiped) to 95.1% (maximum likelihood).

Table 4 shows the overall mean accuracies of each classification method for the differently fed broiler carcasses. The maximum likelihood classifier and the spectral angle mapper both performed with higher accuracy than the other classifiers in identifying all fecal and ingesta contaminants from differently fed broiler carcasses. For the corn-fed carcasses, the classification accuracies ranged from 64.7% (parallelepiped) to 92.3% (spectral angle mapper). The mean accuracy of the classifiers for milo-fed carcasses was slightly lower than for corn-fed carcasses. The accuracies ranged from 62.9% (binary coding) to 88% (maximum likelihood). For wheat-fed carcasses, the highest mean classification accuracy (91.2%) was also obtained with the maximum likelihood classifier. Among the six supervised classification methods, the best classifier for identifying fecal and ingesta contaminants was the maximum likelihood method (90.2%), followed by spectral angle mapper (89.4%), minimum distance (79.6%), Mahalanobis distance (70.3%), parallelepiped (66.0%), and binary coding (64.5%).

The κ coefficients in table 4 indicate overall agreement of a matrix and account for all the elements in a confusion matrix, which was used to calculate overall accuracy in the table. A κ coefficient of 1 indicates perfect agreement between classification and ground truth data. The κ coefficients confirmed that the optimum classifiers were the spectral angle mapper (0.908) for corn, and maximum likelihood for both milo (0.859) and wheat (0.895), indicating that those classifiers had very good agreement in identifying each contaminant from different diets.

Table 5 is a confusion matrix that represents the pixel-level accuracy of the classification results by comparing the classification results with ground truth regions of interests (ROIs). For the corn-fed carcasses with the spectral angle mapper (table 5a), 28 duodenum pixels out of 30 were classified correctly (93.3%), but 2 pixels were misclassified as ingesta. For cecal contaminants classification, only 38 out of 57 pixels were classified correctly (66.7%), and many pixels were misclassified as colon (12 pixels), ingesta (1 pixels), even as skin (6 pixels). However, colon and skin were classified perfectly. For ingesta, only 2 pixels were misclassified as skin, and all others were classified correctly. The overall classification accuracy was 94.7%.

For the milo-fed carcass with the maximum likelihood method (table 5b), the overall classification accuracy was slightly lower (92.6%). Specifically, in this case, many duodenum pixels were misclassified (20% misclassification rate). Among the 33 cecal contaminant pixels, 26 pixels were classified correctly, and 3 pixels were misclassified as duodenum and 4 pixels as colon. However, most colon contaminants were classified correctly (93.8% accuracy). For the ingesta classification, 4 pixels and only 1 pixel out of 72 actual ingesta-contaminated pixels were misclassified as duodenum and ceca, respectively. In addition, most skin was classified correctly (98.6%); only 1 pixel was classified as ceca and 2 pixels as colon.

For the wheat-fed carcass with the maximum likelihood method (table 5c), all 42 pixels of duodenum and 191 pixels of skin were classified correctly; however, 2 cecal pixels out of 49 pixels were misclassified as colon. For the colon classification, 22 pixels out of 35 actually contaminated pixels were classified correctly. However, 9 pixels and 4 pixels were misclassified as ceca and ingesta, respectively. Finally, 54 pixels out of 69 actual contaminated pixels were classified as ingesta, and 12 pixels were misclassified as duodenum and 3 pixels as colon, which resulted in 92.2% overall classification accuracy.

Table 3. Accuracy of classification methods used to classify three different feces and ingesta contaminants on wheat-fed broiler carcasses.

	Sample Examined								
Method[a]	W1606f	W1620f	W1644f	W1653f	W1656f	W1668f	W1677f	W1689f	W1690f
Par	47.38	61.80	63.21	79.19	69.32	79.59	62.88	71.01	67.35
Min	73.60	77.68	65.54	85.91	75.94	88.10	85.60	86.39	84.90
Mah	59.27	71.67	60.10	76.51	64.46	67.01	83.16	77.12	82.65
Max	**80.94**	90.99	**91.45**	**94.30**	90.73	**94.90**	**93.31**	88.76	**95.10**
Sam	72.38	**91.20**	81.87	89.26	**94.26**	94.22	90.87	**91.52**	92.24
Bin	51.40	69.96	61.66	74.83	68.43	57.82	61.66	62.52	65.92

[a] Par = parallelepiped, Min = minimum distance, Mah = Mahalanobis distance, Max = maximum likelihood, Sam = spectral angle mapper, and Bin = binary coding.

Table 4. Mean accuracy of classification methods to classify feces and ingesta contaminants on differently fed (corn, milo, and wheat) broiler carcasses (κ coefficient values given in parentheses).

Method	Corn	Milo	Wheat	Average
Parallelepiped	64.70 (0.590)	66.48 (0.612)	66.86 (0.615)	66.01 (0.606)
Minimum distance	79.73 (0.760)	78.75 (0.747)	80.41 (0.767)	79.63 (0.758)
Mahalanobis distance	69.21 (0.634)	70.41 (0.649)	71.33 (0.659)	70.32 (0.647)
Maximum likelihood	91.44 (0.899)	**88.02 (0.859)**	**91.16 (0.895)**	**90.21 (0.884)**
Spectral angle mapper	**92.27 (0.908)**	87.34 (0.849)	88.65 (0.865)	89.42 (0.874)
Binary coding	66.83 (0.607)	62.94 (0.563)	63.80 (0.574)	64.52 (0.581)

Table 5. Confusion matrix to classify contaminants (duodenum, ceca, colon, and ingesta) from three different feeds (corn, milo, and wheat) on broiler carcasses with optimum classification methods.

(a) Corn			Actual (pixels)					
			Duodenum	Ceca	Colon	Ingesta	Skin[a]	Total
		Duodenum	**28**	0	0	0	0	28
		Ceca	0	**38**	0	0	0	38
	Predicted	Colon	0	12	**49**	0	0	61
	(pixels)	Ingesta	2	1	0	**59**	0	62
		Skin	0	6	0	2	**239**	247
		Total	30	57	49	61	239	436
			Classification accuracy = 94.7%; Classification method = spectral angle mapper					
(b) Milo			Actual (pixels)					
			Duodenum	Ceca	Colon	Ingesta	Skin[a]	Total
		Duodenum	56	3	0	4	0	63
		Ceca	0	26	1	1	1	29
	Predicted	Colon	0	4	30	0	2	36
	(pixels)	Ingesta	14	0	0	67	0	81
		Skin	0	0	1	0	210	211
		Total	70	33	32	72	213	420
			Classification accuracy = 92.6%; Classification method = maximum likelihood					
(c) Wheat			Actual (pixels)					
			Duodenum	Ceca	Colon	Ingesta	Skin[a]	Total
		Duodenum	**42**	0	0	12	0	54
		Ceca	0	**47**	9	0	0	56
	Predicted	Colon	0	2	**22**	3	0	27
	(pixels)	Ingesta	0	0	4	**54**	0	58
		Skin	0	0	0	0	**191**	191
		Total	42	49	35	69	191	386
			Classification accuracy = 92.2%; Classification method = maximum likelihood					

[a] Skin includes image pixels of breast, leg, and wing.

Conclusion

According to the previous report (Park et al., 2003a), a hyperspectral imaging system with simple image processing algorithms could effectively detect fecal and ingesta contaminants on the surface of broiler carcasses. Further analyses of hyperspectral imagery enable us to identify the type and sources of various contaminants (duodenum, ceca, colon, and ingesta) to determine critical control points to improve HACCP for federal poultry safety programs. In this study, six widely used supervised classification methods (parallelepiped, minimum distance, Mahalanobis distance, maximum likelihood, spectral angle mapper, and binary coding) were evaluated for identifying surface contaminants on broiler carcasses. The classification accuracies varied with the methods of classification as well as with the type of feed used to grow the broilers. The mean classification accuracies ranged from 62.9% (binary coding classifier) for milo-fed carcasses to 92.3% (spectral angle mapper classifier) for corn-fed carcasses. However, the maximum likelihood and spectral angle mapper methods performed slightly better than the other methods for all three different diets. The highest classification accuracy was 82% with the maximum likelihood method for milo-fed carcasses, and 91.2% accuracy was obtained for wheat-fed carcasses when the same classification method was applied. The overall classification accuracy obtained in this study for classifying fecal and ingesta contaminants was 90.2%.

For this initial study of the classification methods examined, the parameter values of each classifier were not fully evaluated. Therefore, more investigations are needed to determine the optimum parameter values, such as standard deviation threshold (parallelepiped), distance threshold (minimum distance), probability threshold (maximum likelihood), direction-sensitive distance threshold (Mahalanobis distance), maximum angle in radians (spectral angle mapper), and minimum match threshold (binary coding). Especially, optimum threshold value selection for the Mahalanobis distance method could decrease false positives as well as improve the classification accuracy. When optimum parameter values are determined, all unclassified information can be removed and assigned to a predetermined classification category. In addition, other potential classifiers such as neural networks and fuzzy logic need to be investigated to find better classification methods. Finally, the spectral resolution used for the hyperspectral imagery in this study was less than 1 nm, and each hyperspectral image contained 512 bands, which might be redundant for classification data. Therefore, the optimum number of bands needs to be selected to minimize classification processing time and maximize classification accuracy.

References

Arnoldussen, M. E., D. Cohen, G. H. Bearman, and W. S. Grundfest. 2000. Consequences of scattering for spectral imaging of turbid biologic tissue. *J. Biomed. Optics* 5(3): 300-306.

Bostater, C. R. 1998. Imaging derivative spectroscopy for vegetation dysfunction assessments. *Proc. SPIE* 3499: 277-285.

Burman, J. A. 1999. Hybrid pattern recognition method using evolutionary computing techniques applied to the exploitation of

hyperspectral imagery and medical spectral data. *Proc. SPIE* 3871: 348-357.
Delwiche, S. R., and M. S. Kim. 2000. Hyperspectral imaging for detection of scab in wheat. *Proc. SPIE* 4203: 13-20.
Dwyer, P. J., and C. A. DiMarzio. 1999. Hyperspectral imaging for dermal hemoglobin spectroscopy. *Proc. SPIE* 3752: 72-82.
Feyaerts, F., P. Poller, L. van Gool, and P. Wambacq. 1999. Hyperspectral image sensor for weed selective spraying. *Proc. SPIE* 3897: 193-203.
FSIS. 1997. The Food Safety Initiative's Report to the President, May 1997. Washington, D.C.: USDA Food Safety and Inspection Service.
Hart, C. L., W. J. Slough, and J. B. Rafert. 1998. A review of hyperspectral imagers and comparison with respect to real-time processing on space and aircraft platforms. *Proc. SPIE* 3389: 139-149.
Huebschman, M. L., R. A. Schultz, and H. R. Garner. 2002. Characteristics and capabilities of the hyperspectral imaging microscope. *IEEE Eng. in Med. and Bio.* 21(4): 104-117.
Inoue, Y., J. Penuelus, Y. Nouevllon, and M. S. Moran. 2001. Hyperspectral reflectance measurements for estimating eco-physiological status of plants. *Proc. SPIE* 4151: 153-161.
Kim, M. S., Y. R. Chen, and P. M. Mehl. 2001. Hyperspectral reflectance and fluorescence imaging system for food quality and safety. *Trans. ASAE* 44(3): 721-729.
Kurse, F. A., A. B. Lefkoff, J. B. Boardman, K. B. Heidebrecht, A. T. Shapiro, P. J. Barloon, and A. F. H. Goetz. 1993. The spectral image processing system (SIPS)-interactive visualization and analysis of imaging spectrometer data. *Remote Sensing Environ.* 44(1): 145-163.
Lawrence, K. C., B. Park, W. R. Windham, and C. Mao. 2003. Calibration of a pushbroom hyperspectral imaging system for agricultural inspection. *Trans. ASAE* 46(2): 513-521.
Levenson, R. M., E. S. Wachman, W. Niu, and D. L. Farkas. 1998. Spectral imaging in biomedicine: A selective overview. *Proc. SPIE* 3438: 300-312.
Lu, R., Y. R. Chen, B. Park, and K. H. Choi. 1999. Hyperspectral imaging for detecting bruises in apples. ASAE Paper No. 993120. St. Joseph, Mich.: ASAE.
Malkoff, D. B., and W. R. Oliver. 2000. Hyperspectral imaging applied to forensic medicine. *Proc. SPIE* 3920: 118-128.
Mazer, A. S., M. Martin, M. Lee, and J. E. Solomon. 1988. Image processing software for imaging spectrometry analysis. *Remote Sensing Environ.* 24(1): 201-210.
Park, B., K. C. Lawrence, W. R. Windham, and R. J. Buhr. 2003a. Hyperspectral imaging for detecting fecal and ingesta contaminants on poultry carcasses. *Trans. ASAE* 45(6): 2017-2026.
Park, B., K. C. Lawrence, W. R. Windham, D. P. Smith, and P. W. Feldner. 2003b. Machine vision for detecting internal fecal contaminants of broiler carcasses. ASAE Paper No. 033051. St. Joseph, Mich.: ASAE.
Polder, G., G. W. A. M. van der Heijden, and I. T. Young. 2000. Hyperspectral image analysis for measuring ripeness of tomatoes. ASAE Paper No. 003089. St. Joseph, Mich.: ASAE.
Richards, J. A., and X. Jia, 1999. *Remote Sensing Digital Image Analysis.* Berlin, Germany: Springer-Verlag.
Schowengerdt, R. A. 1997. *Remote Sensing: Models and Methods for Image Processing.* San Diego, Cal.: Academic Press.
Spillman, W. B., Jr., K. E. Meissner, S. C. Smith, S. Conner, and R. O. Claus. 2001. Cellular automata for the analysis of biomedical hyperspectral images. *Proc. SPIE* 4259: 29-35.
Tsuta, M., J. Sugiyama, and Y. Sagara. 2002. Near-infrared imaging spectroscopy based on sugar absorption for melons. *J. Agric. Food Chem.* 50(1): 48-52.
USDA. 1996. Pathogen reduction; hazard analysis and critical control point (HACCP) systems: Final rule. *Federal Register* 61: 38805-38855.
Willoughby, C. T., M. A. Folkman, and M. A. Figueroa. 1996. Application of hyperspectral imaging spectrometer systems to industrial inspection. *Proc. SPIE* 2599: 264-272.
Windham, W. R., K. C. Lawrence, B. Park, and R. J. Buhr. 2003. Visible/NIR spectroscopy for characterizing fecal contamination of chicken carcasses. *Trans. ASAE* 46(3): 747-751.
Zuzak, K. J., M. D. Schaeberle, and E. N. Lewis. 2002. Visible reflectance hyperspectral imaging: Characterization of a noninvasive in vivo system for determining tissue perfusion. *Anal. Chem.* 74(9): 2021-2028.